Lecture 10.

Applications of passive remote sensing:

Remote sensing of precipitation and clouds.

1. Classification of remote sensing techniques to measure precipitation.
2. Visible and infrared remote sensing techniques to measure precipitation.
3. Sensing precipitation in the microwave region.
4. Cloud detection methods. MODIS cloud mask.
5. Retrievals of cloud properties from passive remote sensing: Example of MODIS.

Required reading:

S: 7.4, 6.6, 7.6, 7.7

Additional/advanced reading:

GOES Imager tutorial:
http://rammb.cira.colostate.edu/training/tutorials/goes_8/table_of_contents.asp
Microwave Surface and Precipitation Products System:
http://www.orbit.nesdis.noaa.gov/corp/scsb/mspps/main.html
Future Global Precipitation Measurement (GPM) mission: http://gpm.gsfc.nasa.gov/
MODIS Cloud products: http://modis-atmos.gsfc.nasa.gov/MOD06_L2/index.html
MODIS ATBD Discriminating Clear Sky from Cloud:
http://modis.gsfc.nasa.gov/data/atbd/atbd_mod06.pdf
MODIS ATBD cloud products: http://modis-atmos.gsfc.nasa.gov/_docs/atbd_mod05.pdf

Baum, B. A., and S. Platnick, 2006: Introduction to MODIS cloud products:
http://modis-atmos.gsfc.nasa.gov/reference/docs/Baum_and_Platnick_2006.pdf
Platnick, S., et al., 2003: The MODIS cloud products: Algorithms and examples from Terra. *IEEE Trans. Geosci. Remote Sens.*, **41**, 459-473.
http://modis-atmos.gsfc.nasa.gov/reference/docs/Platnick_et_al._(2003).pdf

Advanced reading:

NOAA's Role in Space-Based Global Precipitation Estimation and Application (2007)
http://books.nap.edu/openbook.php?record_id=11724&page=11

1. Classification of remote sensing techniques to measure precipitation.

- ✓ Only a small fraction of clouds produces rain => need to separate raining from nonraining clouds

Classification of remote sensing techniques:

- Passive remote sensing:
  (i) Visible and infrared techniques
  (ii) Microwave techniques
- Active remote sensing :
  Radar (e.g., TRMM radar)

Other techniques to measure precipitation:

Meteorological Weather Stations (rain gauges)

2. Visible and infrared remote sensing techniques to measure precipitation.

Basic principles:

Clouds are not transparent in the IR and visible (i.e., rain drops can not be sensed directly), thus the approach is to relate independent measurements of rainfall to the properties of a cloud measured by IR and visible remote sensing (called **indirect** measurements of precipitation).

Main problem: a lack of ground truth data to establish a reliable correlation between satellite data and rainfall.

Techniques:

- ➢ Cloud Indexing:

developed by Barrett (1970)

Principle: assign a rate rain to each cloud type

$$Rr = \sum_i r_i \ f_i \qquad [10.1]$$

where $\boldsymbol{Rr}$ is the rainfall rate, $\boldsymbol{r_i}$ is the rain rate assigned to cloud type i , $\boldsymbol{f_i}$ is the fraction of time (or fraction of area covered) by cloud type i.

- Cloud Visible Reflection:

developed by Kilonsky and Ramage (1970)

Principle: tropical oceanic rainfall dominates by deep clouds which are highly reflective in the visible. Highly reflective clouds are more likely to precipitate that "darker" clouds because reflection is related to optical depth and hence to cloud thickness => thus the approach is relate the frequency of highly reflective clouds to precipitation.

Parameterization by Garcia (1981) for tropical oceanic rainfall

$$Rr = 62.6 + 37.4N_D \qquad [10.2]$$

Rr is the monthly rainfall (in mm), $\boldsymbol{N_d}$ is the number of days during the month that the location was covered by highly reflective clouds (e.g., analysis of GOES visible channel).

- OLR (outgoing longwave radiation):

developed by Arkin (1979) to estimate precipitation for climatological studies.

Principle: clouds that are cold in the IR are more likely to precipitate than warm clouds because cold clouds have higher tops (exception, cirrus clouds).

Example: GOES Precipitation Index (GPI) for the tropical Atlantic: $GPI = 3A_c t$

where GPI is the mean rainfall (in mm), $\boldsymbol{A_c}$ is the fractional area (unitless, from 0 to 1) of cloud colder that 235 K in 2.5^0x2.5^0 box, and ***t*** is the time period (hours) for which $\boldsymbol{A_c}$ is determined.

Problems: hard to distinguish "thick" cirrus (nonraining) clouds from deep convective clouds

- Bispectral techniques:

Principle: clouds that have the high probability to produce rain are both **cold** (IR brightness temperature) and **bright** (high reflection in visible).

Example: GOES Multispectral Rainfall Algorithm (GMSRA)

GMSRA combines multispectral measurements of several cloud properties to screen out nonraining clouds: cloud-top temperatures, effective radii of cloud particles and spatial and temporal temperature gradients (see below)

- Cloud model techniques:

Principle: use cloud models to relate satellite visible and IR observations to precipitation.

3. Sensing precipitation in the microwave region.

Advantages:

- microwave radiation penetrates clouds because cloud droplets only weakly interact with microwave radiation, while rain-size drops interact strongly with microwave radiation

Disadvantages:

- microwave radiometers have poor spatial resolution
- contamination from ice crystal scattering

Main principles:
Ice crystals scatter but do not absorb microwave radiation. Rain liquid drops both scatter and absorb, but absorption dominates => relate the optical depth associated with the emitting rain drops and brightness temperature measured by a passive microwave radiometer.

Recall the Marshall-Palmer precipitation size distribution (see Eq.[4.34], Lecture 4)

$$N(r) = N_0 \exp(-2\Lambda\ r)$$

where $N_0 = 8 \times 10^3 m^{-3} mm^{-1}$, but, in general, N_0 depends on the rain type;

$\Lambda = 4.1\ Rr^{-0.21}\ mm^{-1}$, Rr is the rainfall rate (mm/hour).

Thus the volume extinction coefficient is

$$k_{e,rain} = N_0 \int_{r_1}^{r_2} \pi r^2 Q_e \exp(-2\Lambda r) dr \qquad [10.3]$$

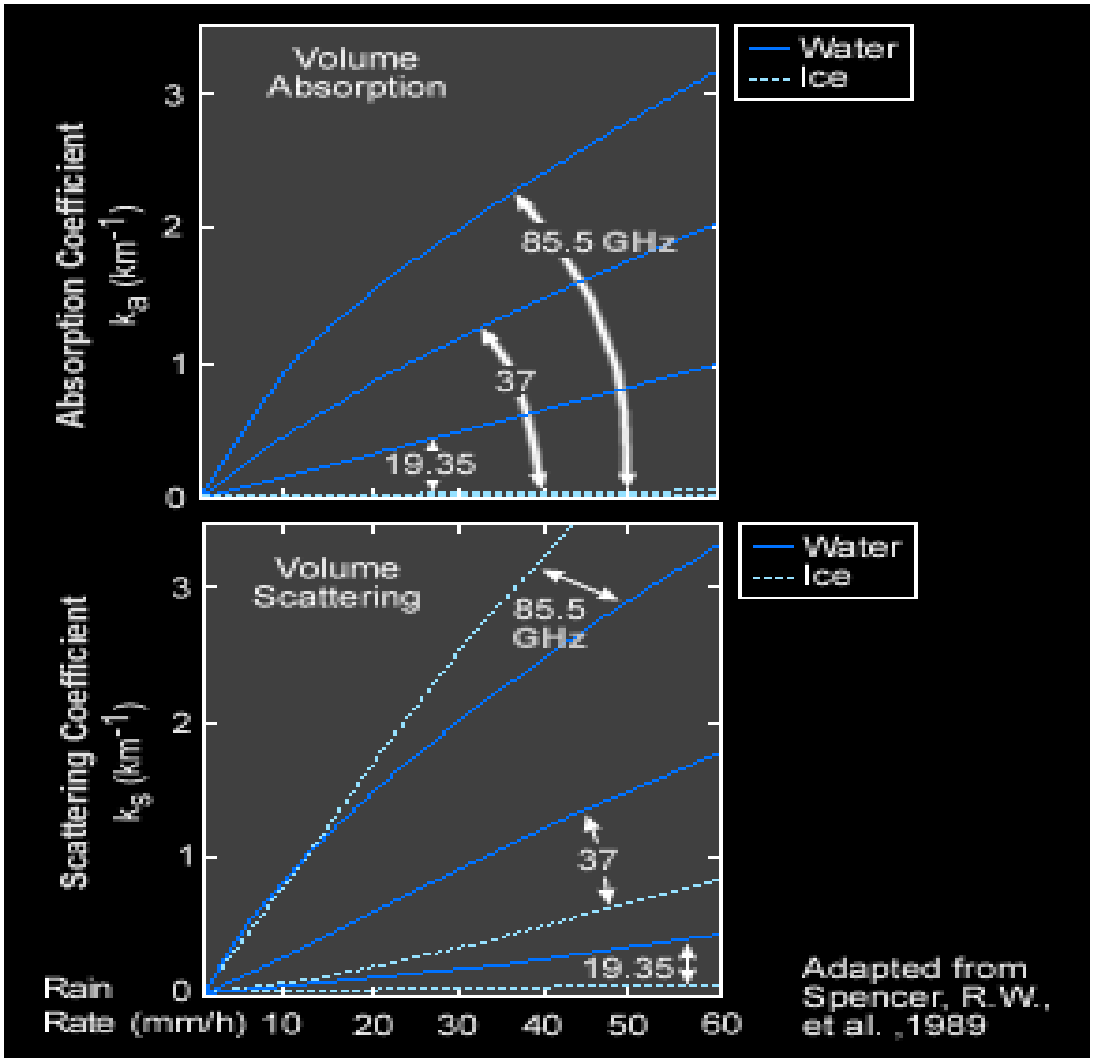

Figure 10.1 Volume absorption (top) and scattering coefficients (bottom) calculated with Mie theory for the Marshall-Palmer precipitation size distribution of water and ice spheres at three frequencies 19.35, 37, 85.5 GHz).

Recall the radiative transfer equation in the microwave region (Lecture 9)

$$T_{b,\tilde{\nu}} = \varepsilon_{\tilde{\nu}}^{p} T_{sur} \exp(-(\tau^{*}/\mu) + \int_{0}^{\tau^{*}} T_{atm}(\tau') \exp(-\tau'/\mu) d\tau'/\mu$$

$$+ R_{\tilde{\nu}}^{p} \exp(-\tau^{*}/\mu) \int_{0}^{\tau^{*}} T_{atm}(\tau') \exp(-(\tau^{*} - \tau')/\mu) d\tau'/\mu$$

Let's assume that T_{atm} is constant in the rain layer and that the volume absorption coefficient is nearly zero, except the rain layer.

$$\int_0^{\tau^*} T_{atm}(\tau')\exp(-\tau'/\mu)d\tau'/\mu \approx T_{atm}[1-\exp(-\tau^*/\mu)]$$

We can re-write the above equation for the microwave brightness temperature observed by a nadir looking microwave radiometer in the following form

$$\begin{aligned} T_{b,\tilde{\nu}} &= \varepsilon_{\tilde{\nu}}^{p} T_{sur}\exp(-\tau^*) + T_{atm}[1-\exp(-\tau^*)] \\ &+ (1-\varepsilon_{\tilde{\nu}}^{p})\exp(-\tau^*)T_{atm}\exp(-\tau^*) \end{aligned} \qquad [10.4]$$

where τ^* is the optical depth associated with the emitting/absorbing rain drops:

$\tau^* = k_{a,rain}\, z_{rain}$

where z_{rain} is the depth of the rain layer.

Re-arranging the terms in the above equation, we have

$$T_{b,\tilde{\nu}} = T_{atm}[1+\varepsilon_{\tilde{\nu}}^{p}(\frac{T_{sur}}{T_{atm}}-1)\exp(-\tau^*) - (1-\varepsilon_{\tilde{\nu}}^{P})(\exp(-\tau^*))^2] \qquad [10.5]$$

Eq.[10.5] helps to understand the brightness temperature-rain rate relationships:

- No rain ($\tau^* = 0$) => $T_{b,\tilde{\nu}} = \varepsilon_{\tilde{\nu}}^{p} T_{sur}$

  (ε is small for water surfaces, and $\varepsilon = 0.9$ for dry land)

- Rain increases (***τ^* increases)*** => $T_{b,\tilde{\nu}} \rightarrow T_{atm}$ Therefore, over water surfaces, the brightness temperature strongly increases with increasing rain rate => raining areas are easily detected over the oceans

  => over the dry land, the changes in brightness temperature are small with increasing rain rate: not useful for rainfall estimations.

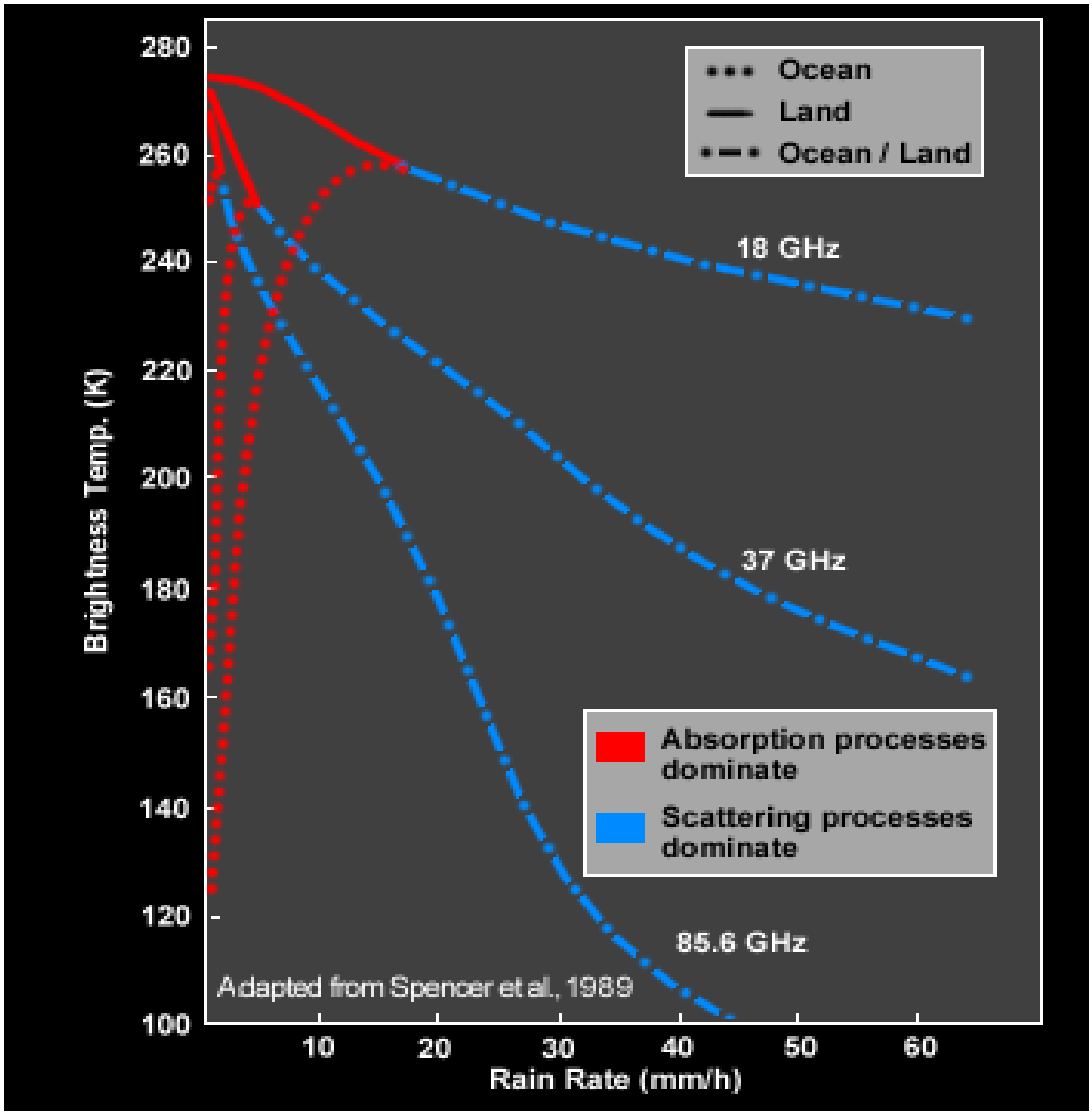

Figure 10.2 Brightness temperature vs. rain rate for three frequencies.

Examples: NOAA MSPPS (Microwave Surface and Precipitation Products System) project:

Operational algorithms for retrieving rain rate:

http://www.star.nesdis.noaa.gov/corp/scsb/mspps/algorithms.html#ARR

Uses NOAA microwave radiometers: Advanced Microwave Sounding Unit (AMSU)

AMSU-A and AMSU-B: launched on NOAA 15, 1998

AMSU-A: 15-channel cross track scanning microwave radiometer; mixed polarization

AMSU-B: 5-channel cross track scanning microwave radiometer

Table 10.1 Microwave sensing of precipitation: AMSU vs. SSM/I

AMSU Frequency	SSM/I Frequency	Microwave processes	Retrieved product
31 GHz	9 GHz	**Controlled by absorption/emission by cloud water**: - large drops/high water content	cloud water and rainfall over oceans
50 GHz	37 GHz	- medium drops/moderate water content	cloud water and rainfall over oceans
89 GHz	85 GHz	- small drops/low water content	non-raining clouds over oceans
89 GHz	85 GHz	**Controlled by ice-cloud scattering**	rainfall over the land and ocean

Integrated IR and microwave operational algorithms:

Example: NOAA Geostationary Operational Environmental Satellites (GOES):

- **Operational Auto-Estimator (AE):** originally developed by Vicente et al. (1998). It is based on a radar-calibrated relationship between 10.7 μm brightness temperature (BT10.7) and rainfall rate. Time changes in BT10.7 are used to identify nonraining cirrus clouds, while adjustments are made for subcloud evaporation (using the product of the precipitable water (PW) and the low-level relative humidity (RH) and for warm-top convection (by adjusting BT10.7 according to the Eta-derived convective equilibrium level (EL) prior to rain rate computation). Problems with identifying and screening cirrus clouds.
- **Hydro-Estimator (HE):** The Hydro-Estimator (Kuligowski et al. 2003) was developed in response to the need to better screen cirrus. This is done by considering the conditions of the surrounding pixels, rather than only of the pixel itself, when determining the presence and rate of rain. In the former case, pixels with BT above the regional average are considered to be nonraining. Other

changes include separate PW and RH adjustments and a scheme for adjusting the rain rate curves based on the condition of surrounding pixels.

- **Hydro-Estimator with Radar (HE-R):** The HE is run with a radar screen similar to the HE in order to demonstrate the mitigated impact of the radar screen on the HE relative to that on the HE.
- **Self-Calibrating Multivariate Precipitation Retrieval (SCaMPR):** SCaMPR (Kuligowski 2002) is an effort to combine the higher accuracy of microwave rainfall estimates (relative to IR) with the more frequent availability and higher spatial resolution of IR estimates. This is done by using microwave rainfall estimates from the Special Sensor Microwave/Imager (SSM/I) and Advanced Microwave Sounding Unit (AMSU) to calibrate an algorithm that uses GOES IR data and derived parameters as input. Calibrations are performed for both rain/no rain separation (using discriminant analysis) and rainfall rate (using multiple linear regression).
- **GOES Multi-Spectral Rainfall Algorithm (GMSRA):** Unlike the AE and HE, the GMSRA (Ba and Gruber 2001) uses data from all five GOES channels to produce rainfall estimates. The visible data and the difference between BT10.7 and BT6.9 are used to differentiate cirrus from raining clouds, while a combination of BT3.9, BT10.7, and BT12.0 are used during the daytime to retrieve estimates of cloud particle size. Separate probability of precipitation and conditional rain rates have been related to brightness temperature via calibration with radar data, and separate calibrations are used for different parts of the US. The PW*RH adjustment of the AE is also applied to the GMSRA.
- **IR/Microwave Blended Algorithm (Blend):** Contains many features of the AE, but instead of a fixed relationship between IR brightness temperature and rain rate, uses microwave-based rain rates from the Special Sensor Microwave/Imager (SSM/I), Advanced Microwave Sounding Unit (AMSU), and Tropical Rainfall Measuring Mission (TRMM) Microwave Imager (TMI) to perform a real-time recalibration of the brightness temperature-rain rate relationship (Turk et al. 1998).

NOTE: All products derived with the above 6 algorithms have been archived by NOAA.

4. Cloud detection methods. MODIS cloud mask.

Recall that the size distribution of cloud drops is often expressed by a modified gamma function (see Lecture 4)

$$N(r) = \frac{N_0}{\Gamma(\alpha) r_n} \left(\frac{r}{r_n} \right)^{\alpha - 1} \exp(-r / r_n)$$

where $\mathbf{N_0}$ is the total number of droplets (cm^{-3}); $\mathbf{r_n}$ in the radius that characterizes the distribution ; $\boldsymbol{\alpha}$ in the variance of the distribution, and $\boldsymbol{\Gamma}$ is the gamma function.

Recall that the **effective radius** is defined as

$$r_e = \frac{\int \pi r^3 N(r) dr}{\int \pi r^2 N(r) dr}$$

and $\mathbf{r_e = (\alpha + 3)\, r_n}$

Cloud reflectance in the solar spectrum:

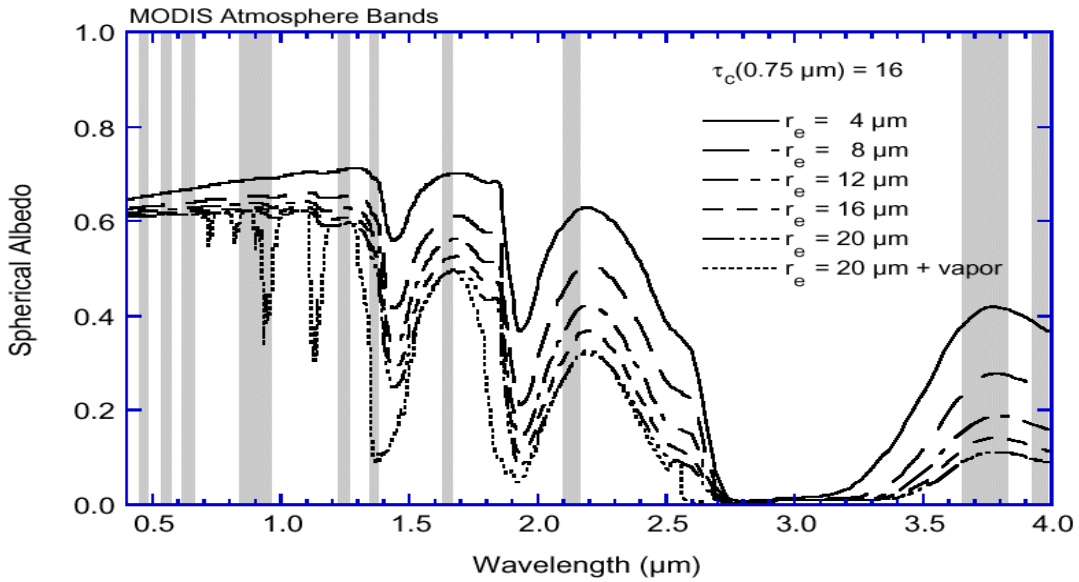

Figure 10.3 Cloud spherical albedo (reflectance) as a function of wavelength for selected values of the effective radius of cloud droplet. Computations were done for a water cloud having a modified gamma size distribution with an effective variance 0.111, cloud optical depth τ_c(0.75 μm)=16, and water vapor content 0.45 g cm^{-2} (ATBD MODIS cloud products). **NOTE**: spherical albedo is defined as $F_{dif}^{\uparrow}(0) / \mu_0 F_0$

IR brightness temperature of clouds:

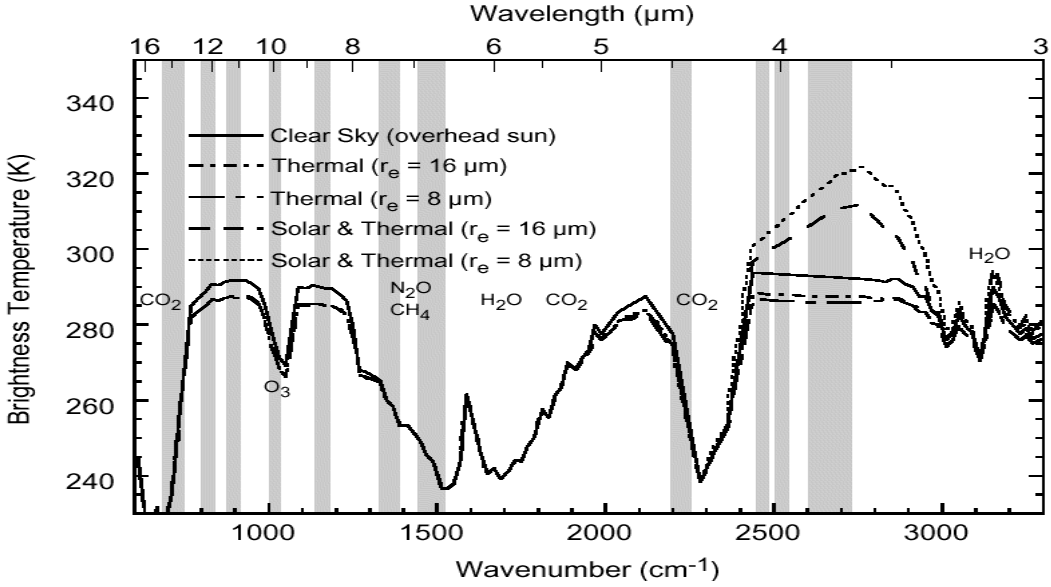

Figure 10.4 Brightness temperature as a function of wavelength (and wavenumber) for nadir observations and selected values of the effective radius of cloud droplets, cloud optical depth τ_c(0.75 μm)=5 for all cases. Computations were done for a water cloud having a modified gamma size distribution for the mid-latitude summer atmosphere with cloud top temperature Tct=14 C, cloud base temperature Tcb=17 C, and blackbody surface temperature Tsur=21 C.

CLOUD DETECTION METHODS:

1. ***Maximum Temperature*** -- all observations of a small surface area over a relatively short period of time are compared. The highest temperature is retained as the best estimate of temperature in that area. This method is based on
   a) ocean surface features are more persistent than clouds
   b) clouds are colder than the surface.
   NOTE: This method works poorly for persistent, thin clouds.
2. ***Two Wavelength Infrared*** -- compare temperatures from 3.7 μm and 10.5 μm (or any pair of wavelengths in the window. If the temperatures are the same, then one can assume the measured signal came from
   a) the sea surface, OR

b) uniform clouds, which will probably be detected in a visual image of the area of interest.

If the temperatures at the two wavelengths are different, then there are scattered, undetected clouds in the scene.

3. ***Infrared Variability*** -- temperatures of clouds tend to be much more variable in space than temperature of the sea surface. Therefore, all areas having a small deviation from a mean brightness temperature close to that expected of the sea in the region are accepted as good values.
4. ***Two Wavelength Visible-Infrared*** -- uses reflected sunlight to detect clouds on the assumption that the sea is much darker in visible wavelengths than clouds.

Table 10.2 General approaches to cloud detection over different surfaces using satellite observations that rely on thresholds for reflected and emitted energy.

Scene	Solar/Reflectance	Thermal	Comments
Low cloud over water	$R_{0.87}$, $R_{0.67}/R_{0.87}$, BT_{11}-$BT_{3.7}$	Difficult. Compare BT_{11} to daytime mean clear-sky values of BT_{11}; BT_{11} in combination with brightness temperature difference tests; Over oceans, expect a relationship between BT_{11}-$BT_{8.6}$, BT_{11}-BT_{12} due to water vapor amount being correlated to SST	Spatial and temporal uniformity tests sometimes used over water scenes; Sun-glint regions over water present a problem.
High Thick cloud over water	$R_{1.38}$, $R_{0.87}$, $R_{0.67}/R_{0.87}$, BT_{11}; $BT_{13.9}$; $BT_{6.7}$ BT_{11}-$BT_{8.6}$, BT_{11}-BT_{12}		
High Thin cloud over water	$R_{1.38}$ $BT_{6.7}$; $BT_{13.9}$ BT_{11}-BT_{12}, $BT_{3.7}$-BT_{12}		For $R_{1.38}$, surface reflectance for atmospheres with low total water vapor amounts can be a problem.
Low cloud over snow	$(R_{0.55} - R_{1.6}) / (R_{0.55} + R_{1.6})$; BT_{11}-$BT_{3.7}$	BT_{11} -$BT_{6.7}$, BT_{13}-BT_{11} Difficult, look for inversions	Ratio test is called, NDSI (Normalized Difference Snow Index). $R_{2.1}$ is also dark over snow and bright for low cloud.
High thick cloud over snow	$R_{1.38}$; $(R_{0.55} - R_{1.6}) / (R_{0.55} + R_{1.6})$;	$BT_{13.6}$; BT_{11} -$BT_{6.7}$, BT_{13}-BT_{11} Look for inversions, suggesting cloud-free.	

Scene	Solar/Reflectance	Thermal	Comments
High thin cloud over snow	$R_{1.38}$; $(R_{0.55} - R_{1.6}) / (R_{0.55} + R_{1.6})$;	$BT_{13.6}$; BT_{11}-$BT_{6.7}$, BT_{13} - BT_{11}	Look for inversions, suggesting cloud-free region.
High Thick cloud over vegetation	$R_{1.38}$, $R_{0.87}$, $R_{0.67}/R_{0.87}$, $(R_{0.87} - R_{0.65}) / (R_{0.87} + R_{0.65})$;	BT_{11}; $BT_{13.9}$; $BT_{6.7}$ BT_{11}-$BT_{8.6}$, BT_{11}-BT_{12}	
High Thin cloud over vegetation	$R_{1.38}$, $R_{0.87}$, $R_{0.67}/R_{0.87}$, $(R_{0.87} - R_{0.65}) / (R_{0.87} + R_{0.65})$;	$BT_{13.9}$; $BT_{6.7}$ BT_{11}-$BT_{8.6}$, BT_{11}-BT_{12}	Tests a function of ecosystem to account for variations in surface emittance and reflectance.
Low cloud over bare soil	$R_{0.87}$, $R_{0.67}/R_{0.87}$, BT_{11}-$BT_{3.7}$; $BT_{3.7}$-$BT_{3.9}$	BT_{11} in combination with brightness temperature difference tests. $BT_{3.7}$-$BT_{3.9}$ BT_{11}-$BT_{3.7}$	Difficult due to brightness and spectral variation in surface emissivity. Surface reflectance at 3.7 and 3.9 μm is similar and therefore thermal test is useful.
High Thick cloud over bare soil	$R_{1.38}$, $R_{0.87}$, $R_{0.67}/R_{0.87}$	$BT_{13.9}$; $BT_{6.7}$ BT_{11} in combination with brightness temperature difference tests.	
High Thin cloud over bare soil	$R_{1.38}$, $R_{0.87}$, $R_{0.67}/R_{0.87}$, BT_{11}-$BT_{3.7}$;	$BT_{13.9}$; $BT_{6.7}$ BT_{11} in combination with brightness temperature difference tests, for example $BT_{3.7}$-$BT_{3.9}$	Difficult for global applications. Surface reflectance at 1.38 μm can sometimes cause a problem for high altitude deserts. For BT difference tests, variations in surface emissivity can cause false cloud screening.

NOTE: R denotes cloud reflectance and BT is brightness temperature of clouds. Index shows the central wavelength of a particular channel.

Example: MODIS Cloud Mask (ATBD Discriminating Clear Sky from Cloud):

- The MODIS Cloud Mask product is a Level 2 product generated at 1-km and 250-m (at nadir) spatial resolutions, day and night.
- MODIS has 250 m resolution in two of the visible bands, 500 m resolution in five visible and near-infrared bands, and 1000 m resolution in the remaining bands. Of

the 36 spectral bands available, 19 visible and infrared radiances are being used in the cloud mask.

- Algorithm based on radiance thresholds in the infrared, and reflectance and reflectance ratio thresholds in the visible and near-infrared

Example of MODIS cloud mask

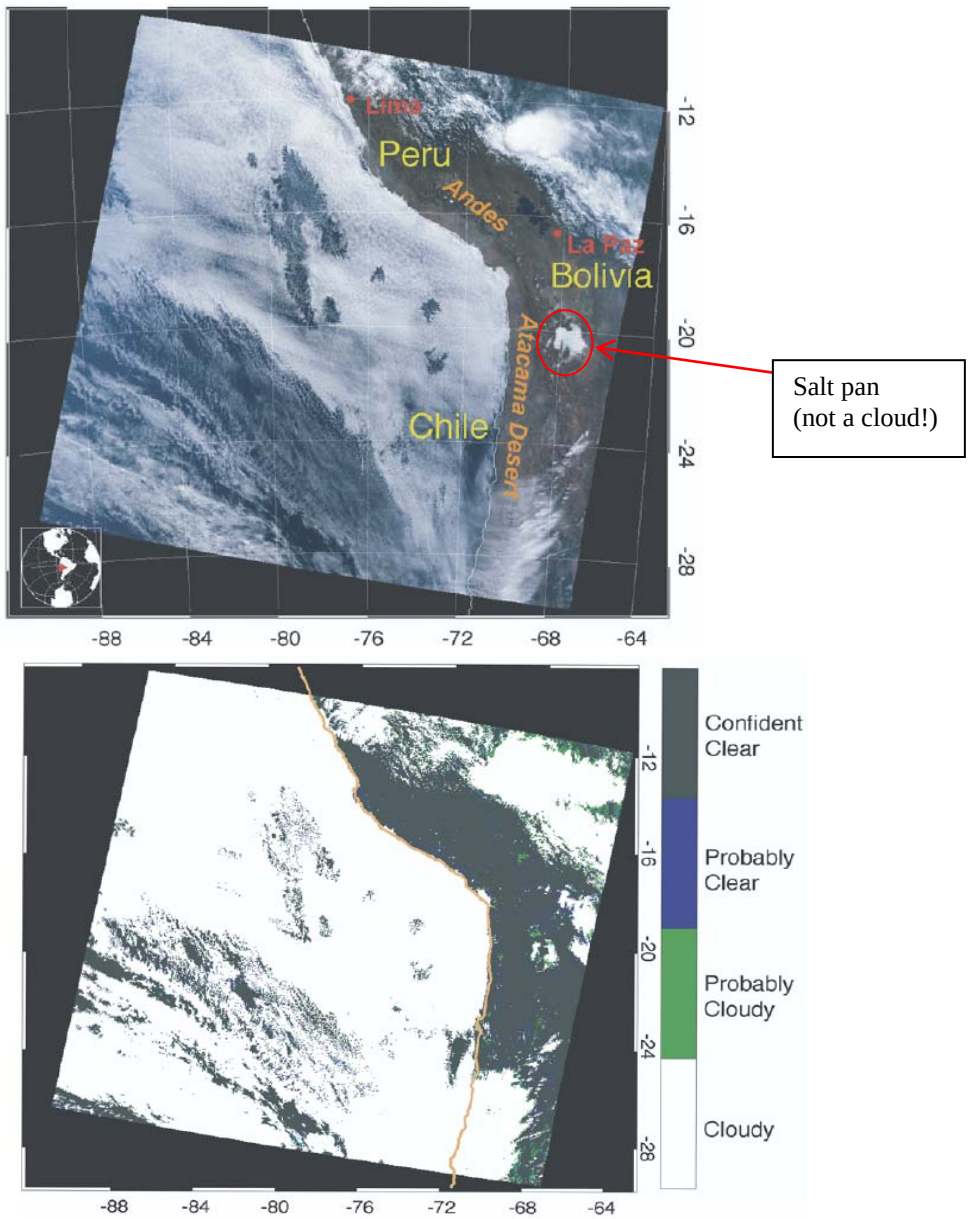

Figure 10.5 True-color image (**upper panel**) of a granule of Terra MODIS data from July 18, 2001, 1530 UTC. The image shows widespread boundary layer stratocumulus clouds off the coasts of Peru and Chile, associated with cool upwelling water along the Humboldt current. Over land clouds overly a variety of surfaces, including coastal deserts, high-altitude ecosystems, and low-land rain forests. **Lower panel**: retrieved cloud mask.

5. Retrievals of cloud properties from passive remote sensing.

Sensors used for cloud remote sensing:

Visible and infrared imagers
Microwave radiometers
Sounders
} **passive sensors**

Active sensors (radars and lidars)

Cloud characteristics retrieved from passive remote sensing data:

a) Cloud detection (cloud presence, amount or cloud fraction)
b) Cloud reflectance (visible imagery)
c) Cloud emissivity (IR imagery)
d) Cloud liquid water content
e) Cloud optical depth
f) Cloud phase (water or ice)
g) Cloud particle size distribution (i.e., effective radius)
h) Cloud-top pressure

Classification of cloud types:

ISCCP classification of cloudy pixel used in remote sensing of clouds

NOTE: ISCCP stands for the International satellite Cloud Climatology Program.

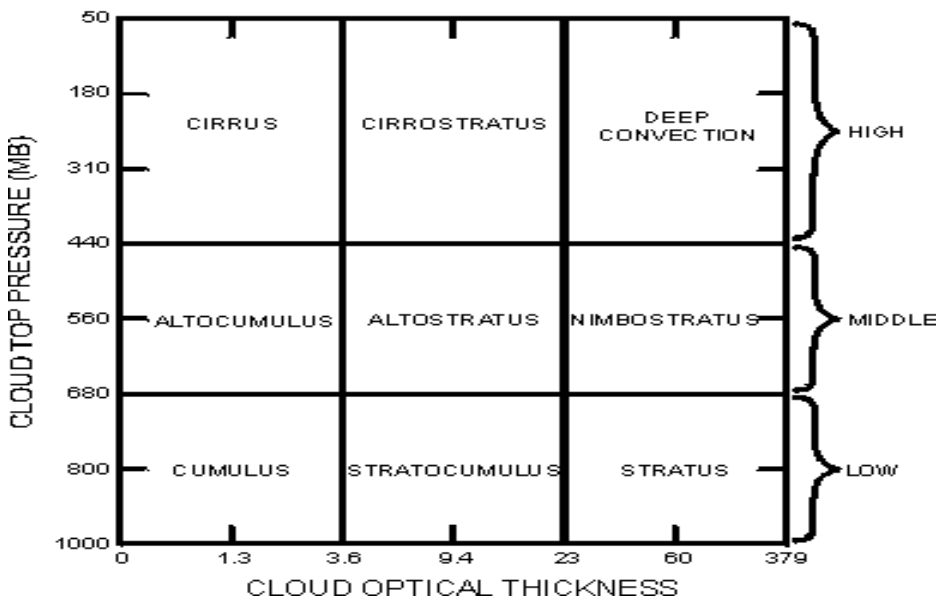

MODIS operational cloud products: include cloud top pressure, thermodynamic phase, optical thickness, particle size, and water path, and are derived globally at spatial resolutions of either 1- or 5-km (referred to as Level-2 or pixel-level products).

Table 10.3 Summary of MODIS Level-2 operational cloud products

Retrieved parameter	Earth Science Data Designation Product ID*	Investigators	MODIS spectral bands used	Spatial resolution (km)	MODIS ancillary input	Non-MODIS ancillary input
CLOUD MASK	**MOD35**	Ackerman *et al.*	up to 20 bands, VIS thru IR	0.25, 1		snow/sea ice mask [a]
CLOUD PROPERTIES	**MOD06**					
CLOUD TOP PROPERTIES						
Cloud-top pressure (p_c), cloud-top temperature (T_c), effective emissivity ($f\varepsilon$)		Menzel *et al.*	11 μm and CO_2 bands (31–36)	5	**MOD35**	model/assimilated T, p profiles [b], SST [c]
CLOUD OPTICAL AND MICROPHYSICAL PROPERTIES:						
Cloud optical thickness (τ_c), particle effective radius (r_e), water path		King *et al.*	VIS, NIR, SWIR, MWIR (bands 1, 2, 5, 6, 7, 20)	1	**MOD35, MOD06** (p_c, T_c), ecosystem + surface albedo[d]	snow/sea ice mask [a], model/assimilated T, p profiles [b], SST [c]
Thermodynamic phase (IR algorithm)		Baum *et al.*	8.5, 11 μm bands (bands 29, 31)	5		

* TERRA DESIGNATION (AQUA IDs ARE MYD35, MYD06, ETC.); NSIDC NISE AND/OR NCEP SEA ICE CONCENTRATION; NCEP GDAS SIX-HOUR DATASET; NCEP REYNOLDS BLENDED SST PRODUCT; AGGREGATION of MODIS ECOSYSTEM CLASSIFICATION PRODUCT (MOD12) WITH MODIS DIFFUSE SKY SURFACE ALBEDO PRODUCT (MOD43) (see Platnick et a.2003)

MODIS cloud products: *cloud top properties*

cloud-top pressure and effective cloud amount or emissivity (product of cloud fraction and cloud emissivity at 11 μm) are retrieved using the CO2- slicing technique (see S:7.7).

NOTE: The CO2- slicing technique has been used in GOES and HIRS.

- ✓ The algorithms is based on differing absorption in several MODIS IR bands located within the broad 15-μm CO2 absorption region, with each band being sensitive to a different level in the atmosphere.

- ✓ Low clouds will not appear at all in the high-absorptions bands, while high clouds appear in all bands. The CO slicing technique has the ability to retrieve cloud pressure and effective cloud amount for opaque or nonopaque mid- to high-level clouds.
- ✓ Cloud height accuracy increases as the observed cloud signal (the clear sky minus the measured radiance) increases for a FOV. For clouds at pressures > 700 hPa (i.e., close to the surface), the cloud signal decreases, thereby precluding application of the method. For low-level clouds, the infrared window 11-μm band temperature is used to determine a cloud-top temperature assuming the cloud is optically thick, and a cloud-top pressure is assigned by comparing the measured brightness temperature to the NCEP Global Data Assimilation System (GDAS) temperature profile.

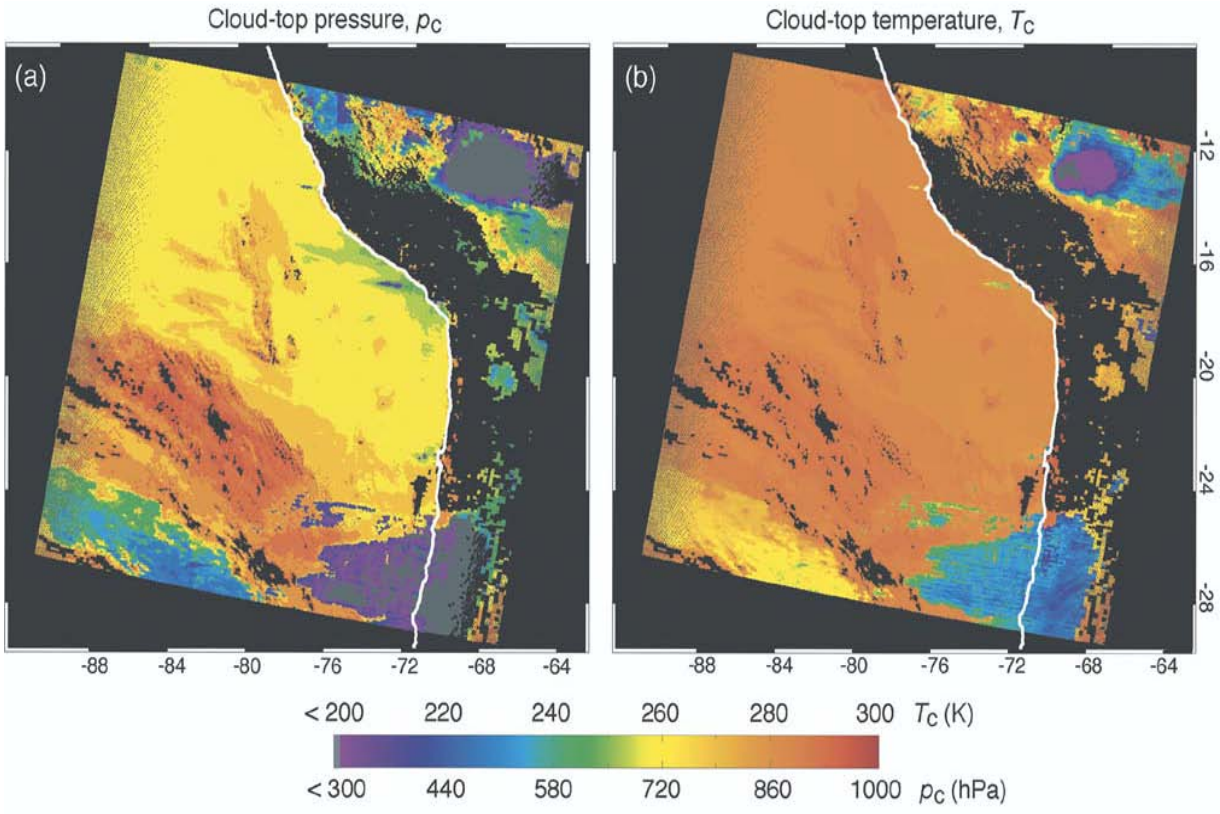

Figure 10.6 (a) Cloud-top pressure and (b) temperature retrievals for the image of Fig. 13.5 (from Platnick et al., 2003)

MODIS cloud products: *Cloud thermodynamic phase*

There are currently three different algorithms:

Bispectral (IR) algorithm*:* uses the inherent difference in water and ice optical constants at 8.52 and 11-μm channels (SDS "Cloud_Phase_Infrared") (see below)

Reflectance algorithm is based on optical constant differences between water and ice in selected shortwave IR (SWIR) bands (1.6, 2.1 μm).

Decision tree algorithm is a logic-based technique that uses results from individual cloud mask tests, as well as IR, SWIR, and cloud-top temperature retrievals. It was developed specifically for the optical thickness and microphysical retrieval algorithm.

NOTE: Results from the latter two phase algorithms are not stored as an SDS but are part of the 1-km pixel-level QA.

Effects of water and ice clouds on solar reflectance and IR brightness temperature:

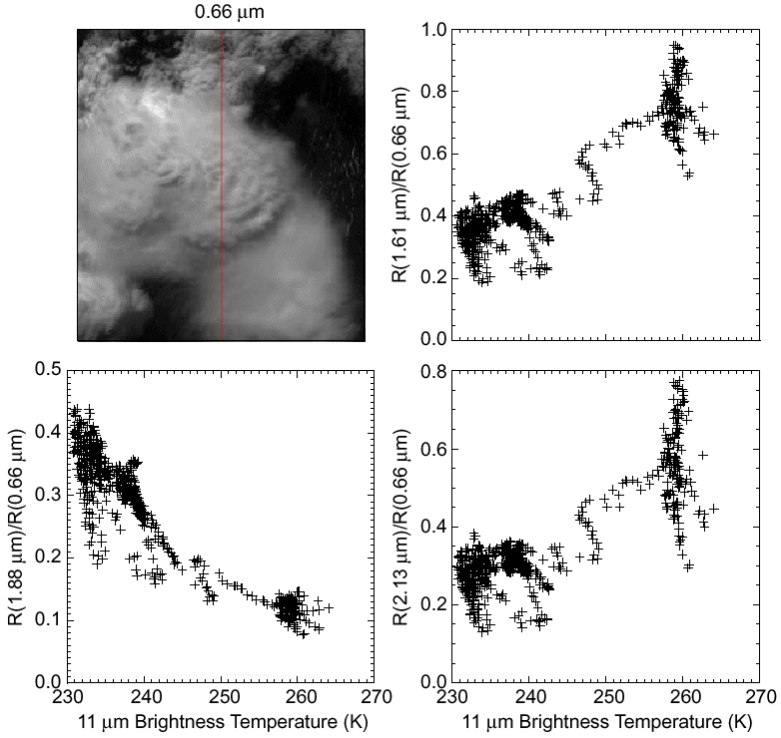

Figure 10.7 The upper left-hand panel shows the 0.66 image from MAS (MODIS airborne simulator) of a convective cumulonimbus cloud surrounded by lower-level water clouds. Subsequent panels show plots of the reflection function ratios as a function of corresponding BT at 11.02 μm. Nadir observations. The MAS 1.88 μm band is the analog for the MODIS 1.38 μm band (King et al., Cloud retrieval algorithm for MODIS). **NOTE**: Ice cloud: low reflectance at 1.61 and 2.13 μm and high reflectance at 1.88 μm

MODIS bispectral algorithm for cloud thermodynamics phase:

- ✓ (Bispectral IR test ($BT_{8.5}$-BT_{11}, BT_{11} thresholds) for both day and night)
- ✓ Uses water/ice emissivity differences in 8.5 μm and 11 μm band:

  differences ($BT_{8.5}$-BT_{11}) tend to be positive and large for ice clouds that have an optical depth > 1;

  $BT_{8.5}$-BT_{11} tend to be small and negative for water clouds of relatively high optical depth ($BT_{8.5}$-BT_{11} is about - 2K);

  $BT_{8.5}$-BT_{11} sensitive to water absorption, so that values become more negative for lower level clouds as the water vapor loading increases, and also as the surface emissivity at 8.5 μm decreases.
- ✓ Possible outcomes: uncertain phase, mixed phase, ice, or liquid water.
- ✓ Known problems:
  - Optically thin cirrus
  - For clouds with cloud-top temperatures of 233-273 K (a mixture of both liquid and ice cloud particles may be present)

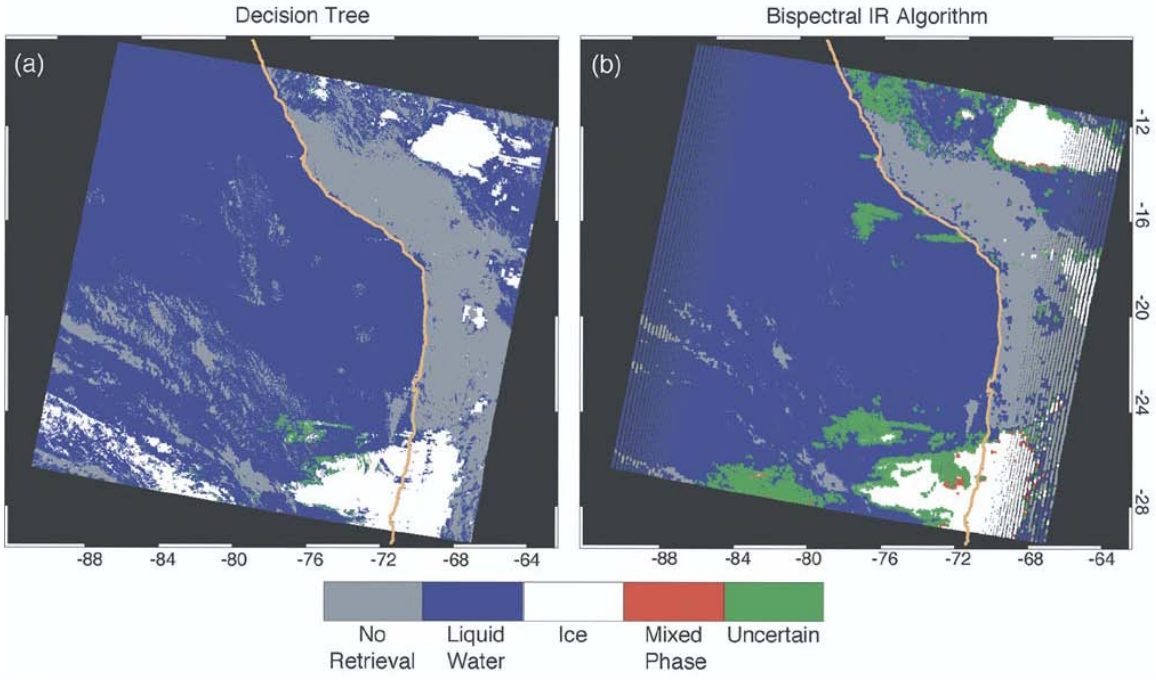

Figure 10.8 Two methods for retrieving cloud thermodynamic phase for the image of Fig. 13.5. (b) Results from the bispectral IR algorithm (8.5- and 11-μm MODIS bands).

The logic of the "decision tree" in (a) is based on results from individual cloud mask tests, the IR and SWIR phase algorithms, and cloud-top temperature retrievals. The decision tree inference is on a 1-km scale while the IR retrieval is at 5 km. The speckled appearance near the scan edge of the IR retrieval image is an artifact of insufficient interpolation to 1-km scales (from Platnick et al., 2003).

MODIS cloud products: *optical thickness and particle size (effective radius):*

Solar reflectance technique:

The reflection function of a nonabsorbing band is primarily a function of optical depth. The reflection function of a near-IR absorbing band is primarily a function of effective radius.

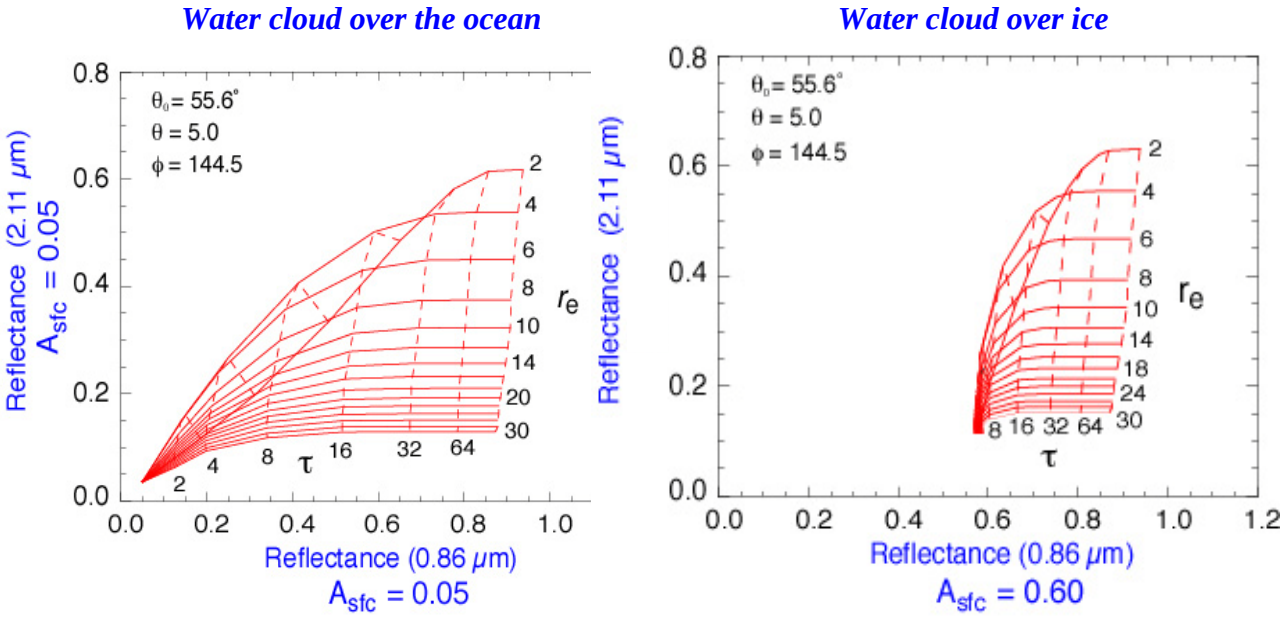

NOTE: here reflectance is defined as $R(\tau_c, \mu, \mu_0, \varphi) = \frac{\pi}{\mu_0 F_0} I^{\uparrow}(0, \mu, \varphi)$

Figure 10.9 Computed reflectance at 2.11 μm channel vs. reflectance at 0.86 μm as a function of cloud optical depth (τ) and effective size r_e: (a) over ocean and (b) over snow. A_{sfc} shows surface albedo.

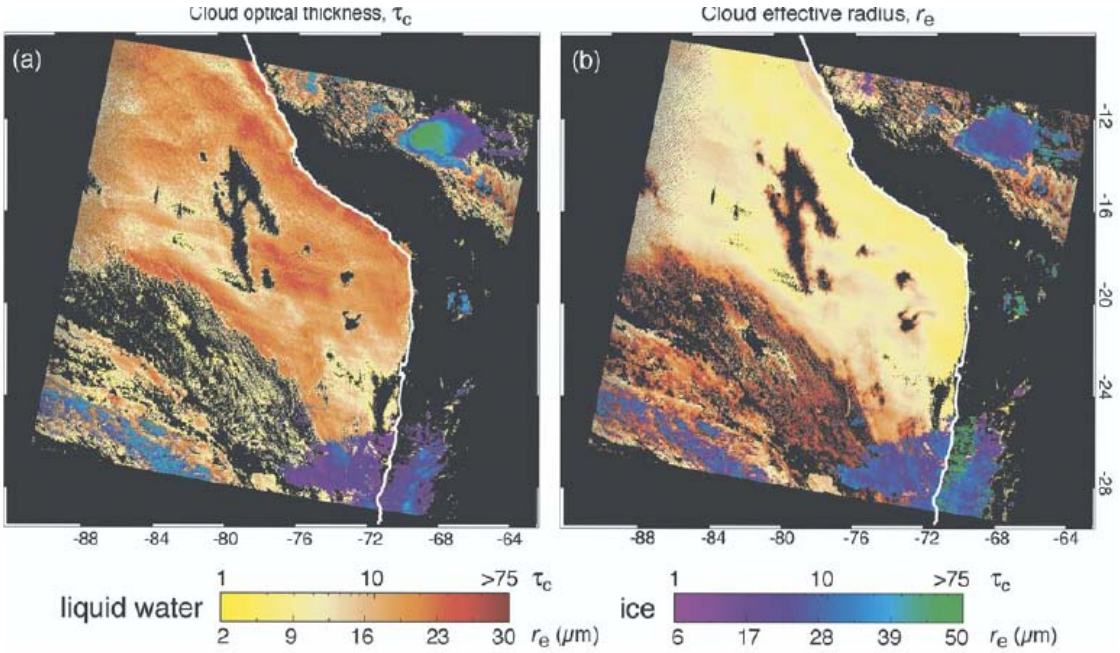

Figure 10.10 (a) Cloud optical thickness and (b) effective particle radius retrievals for the image of Fig. 13.5, with separate color bars for liquid water and ice clouds. Retrievals use the MODIS 2.1-μm band in conjunction with the 0.65-μm band (over land) and the 0.86-μm band (over water) (from Platnick et al., 2003).

MODIS cloud products: optical thickness and particle size (effective radius):

- ✓ 1 km spatial resolution, daytime only, liquid water and ice clouds (using individual cloud mask tests)
- ✓ Solar reflectance technique, VIS through Near-IR (see below)
  –Water nonabsorbing bands: 0.65, 0.86, 1.24 μm
  –Water absorbing bands: 1.6, 2.1, 3.7 μm
- ✓ Retrievals are based are based on library calculations of plane-parallel homogeneous clouds overlying a black surface in the absence of an atmosphere. Separate libraries exist for liquid water and ice clouds, the latter consisting of 12 size distributions composed of four habits (aggregates, bullet rosettes, hollow columns, and plates) with the fraction of each habit depending on particle size. Surface albedo effects and corrections for atmospheric (gaseous) transmittance

are accounted for on a pixel-by-pixel basis. The decision tree approach is used in retrievals.

- ✓ Surface albedo effect.
  - Surface albedo is highly variable spectrally and with surface type.
  - Algorithm uses the MODIS-derived diffuse sky albedo (one of the MODIS standard land products) in connection with IGBP (International Geosphere-Biosphere Programme) land cover classification map.